JOURNAL OF PETROLOGY | VOLUME 43 | NUMBER 9 | PAGES 1707–1724 | 2002

Steady-state Mantle–Melt Interactions in One Dimension: II. Thermal Interactions and Irreversible Terms

P. D. ASIMOW*

DIVISION OF GEOLOGICAL AND PLANETARY SCIENCES, CALIFORNIA INSTITUTE OF TECHNOLOGY, PASADENA, CA 91125, USA

RECEIVED AUGUST 2, 2001; REVISED TYPESCRIPT ACCEPTED MARCH 26, 2002

Progress in development of thermodynamically based models of silicate equilibria with explicit entropy budgets has motivated a reexamination of the conclusion of McKenzie that isentropic upwelling suffices as a model of mantle melting. An entropy budget equation for fractional melting with melt migration in an upwelling two-phase continuum is presented. The energetically self-consistent melt production model predicted by MELTS is used to evaluate numerically the magnitudes of differences between fractional melting (with melt migration) and equilibrium melting (without relative movement) that can be bounded in one dimension: chemical advection by out-of-equilibrium melt; thermal disequilibrium between migrating liquid and residue; frictional dissipation of gravitational potential; dissipation as a result of solid compaction. Like the familiar isobaric case in which fractional melting is significantly less productive than equilibrium melting, chemical isolation of the escaping melts from the residue reduces the oceanic crustal thickness by ∼ 1 km. Allowing escaping melts to move on their own adiabats and ascend at higher temperature than the residue further suppresses melting but yields only ∼ 100 m less crustal thickness. Extra crustal thickness as a result of gravitational dissipation is ∼ 100 m, much smaller than the effect of chemical isolation. Viscous dissipation as a result of compaction is negligible.

KEY WORDS: *isentropic melting; melt migration; dissipation; porous flow; mantle adiabat*

INTRODUCTION

The volumes and compositions of basaltic magmas at mid-ocean ridges and hotspots are an important constraint on the thermal state of the Earth's upper mantle (e.g. Klein & Langmuir, 1987; McKenzie & Bickle, 1988; Asimow *et al*., 2001). Meaningful interpretation of these data, however, requires a thorough understanding of the temperature dependence of the extents of melting produced by mantle processes. Evaluation of the output of decompression melting in these environments usually takes as a reference case the approximation that upwelling and the resulting melting in the mantle are approximately adiabatic processes. There are many types of adiabatic processes, but the starting point of most treatments of mantle melting is that the process is approximately adiabatic and reversible, i.e. isentropic (Verhoogen, 1965; Cawthorn, 1975; McKenzie, 1984; McKenzie & Bickle, 1988; Asimow *et al*., 1995, 1997; Iwamori *et al*., 1995). However, even for the batch melting case where liquid and solid move together, this is only an approximation: for example, thermal diffusion may be negligible, but it is never entirely absent; likewise, there are other sources of entropy production such as chemical diffusion and in the kinetics of chemical reactions, viscous deformation of solid and liquid, and radioactivity (McKenzie, 1984). Moreover, if the liquid phase moves relative to the solid residue, significantly more viscous deformation occurs, the process is no longer reversible because gravitational potential energy is dissipated (Cawthorn, 1975; McKenzie, 1984), the process is no longer locally adiabatic because the liquid can advect heat (McKenzie, 1984), and we must consider the behavior of chemically open systems because disequilibrium will arise between differentially ascending melt and residue (e.g. Spiegelman & Kenyon, 1992). The second law of thermodynamics

*Telephone: (626)395-4133. Fax: (626)568-0935.
E-mail: asimow@gps.caltech.edu

guarantees that the entropy sources as a result of dissipation are positive, but the open-system nature of melt migration processes implies that not all the entropy initially in the system need be available to contribute to melting. The point is that some of these effects will tend to enhance melting relative to the isentropic batch melting case and others will tend to diminish it, and it is an open question as to whether including fully the effects of melt migration leads to more or less melting. Although some of the terms in the entropy balance can be readily dismissed on scaling grounds, others are of comparable magnitude to the isentropic melt production terms and must be evaluated numerically.

A companion paper (Asimow & Stolper, 1999) examined the effects of melt migration on melt production for the case where the liquid remains in both chemical and thermal equilibrium with the residue, a model presumably most applicable to porous flow phenomena. In this paper, I explore the effects of achieving thermal but not chemical equilibrium between flowing melt and surrounding mantle, a situation likely to arise as melt flow becomes channelized or rapid [for a review of rapid melt extraction mechanisms, see Kelemen *et al.* (1997)]. Because thermal diffusion is generally much faster than chemical diffusion [though not necessarily faster than chemical dispersion in porous media, e.g. Schoofs *et al.* (1999)], there is a substantial parameter range for any physical model of melt migration where the melt would be expected to closely approach thermal equilibrium with the surrounding mantle while remaining far from chemical equilibrium with it. In the limiting case considered here, liquids are chemically isolated from the residue as they are produced and mixed with previously extracted liquids, so chemically the one-dimensional process studied is equivalent to accumulated fractional melting. Attention here is focused, however, not on the chemical composition of the liquid but instead on the pressure (P), temperature (T), and extent of melting (F) path dictated by entropy balances in one dimension in this chemically open system.

The entropy balance and its relationship to extent of melting is quantified using MELTS (Ghiorso & Sack, 1995). MELTS provides a self-consistent set of mineral and liquid end-member properties and solution models together with algorithms for the computation of equilibria subject to various thermodynamic constraints, including prescribed bulk composition, P, and total entropy (S). The coupling of chemical and energetic interactions allowed by MELTS calculations has been used to elucidate numerous aspects of magmatic phenomena, including energy-constrained assimilation (Kelemen, 1986; Kelemen & Ghiorso, 1986), isenthalpic melt–rock reaction (Kelemen, 1990), and isentropic decompression (Asimow *et al.*, 1995, 1997, 2001; Hirschmann *et al.*, 1999*a*).

Although melt flow beneath mid-ocean ridges is at least two dimensional (Ahern & Turcotte, 1979; Spiegelman & McKenzie, 1987) and probably includes a significant component of three-dimensional flow (Phipps Morgan & Forsyth, 1988; Parmentier & Phipps Morgan, 1990; Sparks & Parmentier, 1993), one-dimensional calculations provide a simple and useful framework for thinking about more complicated flow regimes. For example, a one-dimensional flow model (i.e. including thermal equilibration, but without melt focusing) probably provides a minimum estimate of the magnitude of heating of the country rock by migrating liquids at the axis of a mid-ocean ridge, as higher dimensional flows are thought to focus more melt to the axis (Spiegelman & McKenzie, 1987). Finally, although there is no reason, *a priori*, to expect that melt extraction is a steady process (Scott & Stevenson, 1989), steady solutions of the sort presented here provide a simple baseline for understanding time-dependent behaviors.

ENTROPY BUDGET AND MELT PRODUCTION: ANALYSIS

A theory for flow of a two-phase (solid plus liquid) continuum with transfer of mass between the phases (i.e. melting), viscous deformation of the solid, and separation of the phases by porous flow was developed and applied to the mantle upwelling problem by McKenzie (1984). For the case where melt and matrix are in both thermal and chemical equilibrium at all levels in the column (i.e. a common temperature and a common chemical potential for every component in both liquid and solid at every depth), McKenzie combined a statement of conservation of momentum consistent with Darcy's law with a statement of the first law of thermodynamics to obtain an equation showing the relative importance of isentropic and irreversible processes. In one dimension and at steady state, McKenzie's entropy equation (A37) can be solved for the melting rate Γ (mass transferred from solid to melt per unit volume and time) and written

$$\Gamma = -\frac{\left[(1-\varphi)\rho_s W\frac{dS_s}{dz} + \varphi\rho_f w\frac{dS_f}{dz}\right]}{(S_f - S_s)} + \frac{\left[\frac{d}{dz}\left(k_T\frac{dT}{dz}\right) + H + \frac{\mu\varphi^2}{k}(w-W)^2 + \left(\zeta+\frac{4}{3}\eta\right)\left(\frac{dW}{dz}\right)^2\right]}{T(S_f - S_s)} \quad (1)$$

where z is the vertical coordinate, T is temperature, S_f and S_s are the specific entropies of the melt and matrix [see Hirschmann *et al.* (1999*a*) for a discussion of the entropy of fusion in multicomponent systems], φ is the volume fraction of melt-filled porosity, ρ_s and ρ_f are solid and melt density, W is the velocity of the solid matrix in the z direction (positive upwards), w is the velocity of the melt, k_Γ is the bulk thermal conductivity, μ is the viscosity of the melt, k is the permeability (a function of φ), ζ is the bulk viscosity and η the shear viscosity of the matrix, and H is the rate of internal heat generation by radioactivity. In practice, use of this equation requires an expression for the extent of melting as a function of T and P and the thermodynamic properties (mixing models, standard entropy, heat capacity, volume, and thermal expansivity) of the phases. The first ratio on the RHS of this equation describes isentropic melting, whereas the second ratio incorporates the effects of entropy production mechanisms within the system. The first quantity in the numerator of the second ratio represents the effects on melt production of thermal diffusion in the z direction [Budiansky (1970) provided a formalism for obtaining bulk thermal diffusivity from the liquid and solid values]; the second describes the effects of radioactive heat production. The third term in the numerator of the second ratio results from relative vertical flow of melt and matrix. In McKenzie's inertia-less approximation, it represents both the frictional losses during porous flow where the pressure drop is given by Darcy's law (Bejan, 1982) and the effect of gravitational potential energy release (which is converted to heat through viscous dissipation in the melt). The fourth and final term in the numerator of the entropy production term describes the effects of viscous compaction of the solid matrix.

Formulation for fractional melt transport

It must be emphasized that although equation (1) and the rest of McKenzie's theory account for melt migration relative to the matrix, they explicitly assume that the melt and matrix are everywhere in thermal and chemical equilibrium. This restriction makes the chemical fluxes equivalent to those of a closed system so that the first law of thermodynamics for the system of melt plus matrix can be written as $\mathrm{d}E = T\mathrm{d}S - P\mathrm{d}(1/\rho)$; i.e. chemical or mass flux terms are not included in the energy balance. If we do not assume melt and matrix to be in thermal and chemical equilibrium, then the first law must be written separately for the melt and solid parts of the system as $\mathrm{d}E_f = T_f\mathrm{d}S_f - P\mathrm{d}(1/\rho_f) + \Sigma\, \mu_f^n \mathrm{d}X_f^n$ and $\mathrm{d}E_s = T_s\mathrm{d}S_s - P\mathrm{d}(1/\rho_s) + \Sigma\, \mu_s^n \mathrm{d}X_s^n$, where T_f and T_s are the (possibly distinct) temperatures of the melt and solid reservoirs, μ_f^n and μ_s^n are the chemical potentials of the nth component in melt and solid (not to be confused with μ without subscript or superscript, which is the viscosity of the melt), and X_f^n and X_s^n are the mass fractions of the nth component in the melt and solid phases. Using these expressions leads to a productivity equation analogous to (1) that can be written

$$\Gamma = \frac{\left\{\begin{array}{ll} -\,T_s\left[(1-\varphi)\rho_s W\dfrac{\mathrm{d}S_s}{\mathrm{d}z} + \varphi\rho_f w\dfrac{\mathrm{d}S_f}{\mathrm{d}z}\right] & \\ -\,(T_f - T_s)\varphi\rho_f w\dfrac{\mathrm{d}S_f}{\mathrm{d}z} & \text{‘A’} \\ -\displaystyle\sum_{n=1}^{N}(\mu_f^n - \mu_s^n)\left(X_f^n\Gamma + \varphi\rho_f w\dfrac{\mathrm{d}X_f^n}{\mathrm{d}z}\right) + & \text{‘C’} \\ \dfrac{\mathrm{d}}{\mathrm{d}z}\left(k_\Gamma\dfrac{\mathrm{d}T}{\mathrm{d}z}\right) + H + \dfrac{\mu\varphi^2}{k}(w-W)^2 + \left(\zeta + \dfrac{4}{3}\eta\right)\left(\dfrac{\mathrm{d}W}{\mathrm{d}z}\right)^2 & \end{array}\right\}}{T_s(S_f - S_s) + \underbrace{S_f(T_f - T_s)}_{\text{‘B’}}} \qquad (2)$$

which contains new terms ‘A’, ‘B’, and ‘C’ that express the effects on the entropy budgets of flow of melt with a different temperature and with a different set of chemical potentials from the matrix. The term ‘A’ in the numerator is due to advection of entropy by liquid moving at a temperature different from the matrix temperature. The extra term ‘B’ in the denominator of equation (2) represent the correction to the entropy of fusion associated with changing (generally, raising) the temperature of new increments of melt as they are transferred at constant pressure from the solid reservoir at T_s to the melt reservoir at T_f. Generally, $T_f > T_s$ because the matrix is cooled by melting, so the extra denominator term leads to less melting than in the isentropic approximation. The new temperature-difference terms arising from melt separation are independent of and appear in addition to the gravitational–frictional term. It is somewhat artificial to separate these two, as adiabatic melting and temperature changes in response to decompression on ascent require a pressure gradient, which in turn ultimately derives from the gravity field, but it remains instructive to take the pressure gradient as given and consider the gravitational–frictional term separately.

The new term ‘C’ in the numerator of (2) that depends on $(\mu_f^n - \mu_s^n)$ accounts for open-system chemical effects, whereby the entropy budget is modified by flow of melt that is out of chemical equilibrium with the residue; it also contains advection and melting subterms. This term captures the energetic consequences of the compositional differences between the equilibrium and fractional melting cases and persists even for the case of thermal equilibrium as long as the liquid and solid are out of chemical equilibrium. Although examination of this term suggests no obvious value for its sign, intuition from simpler batch and fractional melting processes (e.g. isobaric melting) suggests that this term ought to result in the well-known tendency for fractional melting to yield less melt than the equilibrium case (Presnall, 1969), at least at low melt fraction (Asimow *et al.*, 1997; Hirschmann *et al.*, 1999*a*). Its quantitative significance will be evaluated below in the open-system polybaric melt migration case by comparison with the equilibrium porous flow column (Asimow & Stolper, 1999).

Scaling analysis

I will present a numerical approach to evaluating the importance, relative to isentropic flow (i.e. equilibrium melting in which melt migration relative to the residual solids does not occur), of the terms arising from chemical isolation of ascending melt and solid, the degree to which thermal equilibration is achieved, and gravity–friction as a result of flow of the liquid relative to the solid matrix in the context of the MELTS model. The remaining terms (thermal conduction, radioactive heat production, and dissipation by compaction of the matrix) will be evaluated on scaling grounds by comparison with the magnitude of the terms resulting from reversible adiabatic closed-system decompression. Expressed as power available to cause melting per unit volume, the isentropic decompression terms in the numerator of the first ratio on the RHS of equation (1) are of order $\rho W C_p(\partial T/\partial z)$, which is $\sim 3 \times 10^{-6}$ W/m^3 for a thermal gradient in the melting region of 10 K/GPa and an upwelling velocity of 10 cm/yr.

Thermal conduction and radioactive heat production

The thermal conduction term [the first quantity in the numerator of the second ratio on the RHS of equation (1)], given a 10 K/GPa thermal gradient, a characteristic length of 30 km, and a conductivity of 3 W/m K (Hofmeister, 1999), is of order $\sim 3 \times 10^{-8}$ W/m^3. For a source with chondritic abundances of the heat-producing elements, radiogenic heat production is also $\sim 3 \times 10^{-8}$ W/m^3, and a depleted source (e.g. Hofmann, 1988) would be about an order of magnitude lower. Hence we expect that neither of these terms leads to an increase of more than $\sim 1\%$ in the melt production relative to the reference case of purely isentropic (batch) melting. Consequently, these terms will not be considered further.

Gravity and frictional dissipation as a result of relative flow of liquid and solid

Although the magnitude of entropy production from dissipation as a result of vertical separation of melt and residue in a gravity field depends on the relative velocity of melt migration, there is a well-defined upper limit to this term [the third quantity in the numerator of the second ratio on the RHS of equation (1)] for the case of infinite permeability. Using Darcy's law,

$$\varphi(w - W) = -\frac{k}{\mu}\left(\frac{dP}{dz} + \rho_f g\right) \tag{3}$$

(g is the acceleration due to gravity), together with the constraints from conservation of mass flux in one dimension and steady state,

$$(1 - \varphi)\,\rho_s W = (1 - F)\,\rho_s^o W_o \tag{4}$$

$$\varphi \rho_f w = F \rho_s^o W_o \tag{5}$$

where F is the extent of melting by mass and ρ_s^o and W_o are the values at the base of the melting column [equations (7′) and (8′) of Asimow & Stolper (1999)], the term related to relative velocity of melt and matrix can be written in terms of power per unit volume available to cause melting:

$$\Delta H_{gravity} = \left[\frac{\mu\varphi^2(w - W)^2}{k}\right] \tag{6}$$

$$= -\rho_s^o W_o\left[\frac{F}{\rho_f} - \frac{\varphi}{(1-\varphi)}\frac{(1-F)}{\rho_s}\right]\left(\frac{dP}{dz} + \rho_f g\right).$$

The limit of infinite permeability corresponds to $\varphi = 0$, because melt is removed instantaneously as it is produced and migrates at infinite velocity. Furthermore, ignoring dynamic pressures (i.e. assuming hydrostatic equilibrium), in this limit the hydrostatic pressure gradient $dP/dz = -\rho_s g$. Thus we can write a maximum value for the gravitational source term in units of energy per unit volume and time:

$$\Delta H_{gravity} \leq \rho_s^o W_o\left[\frac{F(\rho_f - \rho_s)g}{\rho_f}\right]. \tag{7}$$

In scaling terms for $(\rho_f - \rho_s) \sim 500$ kg m^{-3}, the magnitude of this power source is of order $(1{\cdot}5 \times 10^{-5})F$; that is, it should become of similar magnitude to the isentropic decompression terms at $F \sim 0{\cdot}2$ and hence may be a significant effect for the extents of melting expected in mid-ocean ridge melting columns. Integrated over a whole column, to the extent that g and the densities are nearly constant, the total gravitational power source is proportional to the integral of $F dP$. Because F varies in a non-linear fashion with P in the MELTS model, and the impact of a given entropy source on melt production also varies with P, it is worth examining the effect of this term numerically.

Dissipation as a result of compaction of matrix

Viscous deformation of the solid matrix leads to dissipation and hence entropy production. In multiple dimensions, the solid deformation has components of shear as well as compaction and the dissipation as a result of shear may be significant near the corner of a corner flow under a ridge or above a slab, but in one dimension we can describe only the compaction term. Unlike the gravity term, there is no absolute upper limit to the compaction dissipation, but we can show that it is negligible compared with the gravity term except in the unlikely circumstance that the extent of melting changes dramatically over a scale similar to the compaction length δ_c (McKenzie, 1984), defined as

$$\delta_c = \sqrt{\frac{(\zeta + \frac{4}{3}\eta)k}{\mu}} \tag{8}$$

where $[\zeta + \frac{4}{3}\eta]$ is the compaction viscosity of the solid matrix (a linear combination of shear viscosity η and bulk viscosity ζ), k is the permeability, and μ is the viscosity of the melt.

The source term for dissipation as a result of compaction [the fourth quantity in the numerator of the second ratio on the RHS of equation (1)] can be estimated as follows for the high-permeability case (which is the case with maximum compaction). Equation (3), for $\varphi = 1$ and $\rho_s \approx \rho_s^o$, leads to

$$\frac{dW}{dz} \approx -W_o\frac{dF}{dz} \approx -W_o\frac{\Delta F}{\Delta z} \tag{9}$$

where extent of melting F changes by ΔF across some vertical interval Δz. Hence, using the definition of compaction length (8), the power per unit volume available to cause melting as a result of compaction becomes

$$\Delta H_{\mathrm{compaction}} = (\zeta + \tfrac{4}{3}\eta)\left(\frac{dW}{dz}\right)^2 \approx \frac{\mu}{k}W_o^2\Delta F^2\frac{\delta_c^2}{\Delta z^2}. \tag{10}$$

For $w \gg W$ and $\rho_f \approx \rho_s^o$, equation (4) and Darcy's law give

$$W_oF \approx \varphi w \approx \frac{k}{\mu}(\rho_f - \rho_s)g. \tag{11}$$

Substituting (11) into (10) and using the upper bound from equation (7) gives

$$\begin{aligned}\Delta H_{\mathrm{compaction}} &\approx W_o[F(\rho_f - \rho_s)g]\left(\frac{\Delta F}{F}\right)^2\left(\frac{\delta_c}{\Delta z}\right)^2 \\ &\approx \Delta H^{\max}_{\mathrm{gravity}}\left(\frac{\Delta F}{F}\right)^2\left(\frac{\delta_c}{\Delta z}\right)^2.\end{aligned} \tag{12}$$

Hence the compaction term is significant, relative to the gravitational–frictional term, only over an interval Δz comparable with or smaller than the compaction length δ_c across which $\Delta F/F$ approaches one.

Taking Δz as the whole melting column and $\Delta F = F_{\max}$, for ordinary values of the solid viscosity, melt viscosity, and permeability, the compaction length (~100 m) is orders of magnitude smaller than the height of the melting column (~50 km), and dissipation by compaction is totally negligible. However, if the melting region were to contain a narrow interval over which F changes dramatically, this could be a location of large heating by dissipation. One example would be a discontinuous solidus, where F changes from zero to a finite value over an infinitesimal interval. However, in an adiabatic system even a univariant solidus does not behave this way (Asimow *et al.*, 1997), and F is a continuous function of z across the solidus. The other possibility is a sudden freezing or melting front as a result of a mineral reaction in which melt productivity approaches values of (plus or minus) percent per meter rather than percent per kilometer. In general, oceanic melting regimes contain no such intervals, although the appearance of residual plagioclase may cause a sudden freezing front in regions of very low potential temperature (Asimow *et al.*, 1995). Finally, if we relax the assumption $\varphi = 1$, there is the possibility of a sharp transition from high porosity to low porosity as a result of a sudden change in melt migration mechanism, which could generate a compaction front without a sharp change in extent of melting.

In the model compaction problem solved by McKenzie (1984), an interval of finite porosity discontinuously overlies an impermeable lower boundary. The initial solution to this problem generates significant heating by viscous compaction within the resulting compaction boundary layer. However, for normal oceanic melting regimes where melt fraction varies smoothly and changes significantly only over intervals much larger than a compaction length, this dissipation source is much smaller than the gravitational dissipation term, whose maximum effect will be illustrated numerically below.

Terms owing to temperature difference between melt and matrix

McKenzie (1984) gave simple scaling arguments for the relative importance of both the gravitational–frictional entropy source and the heat transfer between migrating liquids and residual mantle, expressed in terms of crustal thickness [for mid-ocean ridge-like geometries, crustal thickness is proportional to the product of mean extent of melting and the thickness of the melting region (Klein & Langmuir, 1987; Plank *et al.*, 1995)]. He concluded that the total amount of extra melting from either source when melt migration occurs (relative to the isentropic case) was comparable with the variations in crustal thickness as a result of either uncertainty in the entropy of fusion or retention of 3% melt in the matrix. McKenzie therefore concluded that isentropic melting sufficed as a minimum estimate and a useful first approximation given the state of knowledge of thermodynamic data and melt migration phenomena at the time.

I emphasize here that the terms in equation (2) containing ($T_f - T_s$) express the principal reason why melt migration, if the liquids move in thermally isolated channels, results in less melting than the case without relative motion of melt and matrix. Specifically, motion of liquid at higher temperature than the surrounding mantle advects heat out of the system. Hence, the first-order effect of removing these terms by forcing thermal equilibrium between the migrating melt and the matrix can only bring the productivity of melting back up towards the value realized by the non-migrating case (although a difference will still remain if chemical disequilibrium occurs; see below). In other words, the fact that temperature differences between adiabatically ascending liquid and melting residues may arise should not be viewed as a source of extra melting owing to melt migration, but as a possible reason why melt migration may lead to less melting than the impermeable case, if the entropy flux carried by the hot liquids is not recovered and allowed to cause melting.

The magnitude of the terms resulting from temperature differences between melt and solid [‘A’ and ‘B’ in equation (2)] may be significant (McKenzie, 1984) and can be examined numerically using a one-dimensional, steady-state fractional melting column as a model. This model is related to the equilibrium porous flow system discussed in the companion paper (Asimow & Stolper, 1999), but in this case, as liquid is produced by melting it is removed from chemical contact with the residual solids and mixed into a separate reservoir containing other increments of liquid extracted at higher pressures. This liquid reservoir, although remaining chemically isolated (except for further inputs of fractional melt), may then be allowed to interact thermally with the residual mantle reservoir. The possible decrease in macroscopic configurational entropy associated with the ‘Maxwell’s Demon’ action of melt segregation into a separate reservoir is ignored, but the entropy production associated with mixing of liquids of different compositions and temperatures is included. The geometrical form of the two reservoirs is not specified; the calculation is intended to describe any model of two-phase flow that, for some choice of parameters, might be characterized by weak chemical interactions and strong thermal interactions between liquid and solid phases. The calculations continue to the base of the igneous crust with no accounting for conduction, as the purpose is not to model lithospheric effects but to test deviations from isentropic behavior in the advection-dominated asthenosphere. Hence, the shallowest part of these calculations will apply only to regions of thin lithosphere such as fast spreading-rate mid-ocean ridges.

As I develop in some detail in subsequent sections, the numerical results show that when considered in terms of the total amount of melt produced by a melting column, McKenzie’s conclusions about the magnitudes of the effects owing to heat transfer between melt and matrix and owing to gravity are correct, although in part for reasons he did not consider, such as the limitation on melting along most normal mantle adiabats imposed by the exhaustion of clinopyroxene. However, it will also be shown that segregated, ascending liquid interacting thermally with the ascending residual column can in some circumstances cross its liquidus and begin to crystallize (releasing latent heat and thereby causing even more melting of the surrounding mantle); this means that deep, sublithospheric fractionation of ascending liquids is possible and that the thermal effects of melt migration can, in principle, lead to changes in the composition and mean pressure of melting (Klein & Langmuir, 1987) of the integrated melt and in the amount of liquid that actually reaches the crust. A general conclusion of these numerical models will be that, even though the entropy sources considered here are small, the overall behavior of multiphase, multicomponent systems in energetically self-consistent calculations can be variable and complex depending on the details of the thermal modeling, and this may contribute to observed variability in natural magmatic systems.

ENTROPY BUDGET AND MELT PRODUCTION: NUMERICAL EXPERIMENTS

The effect of advection of heat by ascending melt can be studied in a straightforward way because at steady state for certain end-member equilibration models it is independent of the rate of melt migration. This is a corollary of the arguments developed by Asimow & Stolper (1999) concerning the relationship between equilibrium porous flow and batch melting. We showed that if there are no source terms for mass or energy, then for the thermal and chemical equilibrium problem described by equation (1), the constraints of one dimension and steady state require that the fluxes of each mass component and of entropy carried by solid and by liquid and hence the chemical composition and temperature of the melt and solid be independent of the relative velocity of melt and matrix. In the steady-state one-dimensional disequilibrium melting problem described by equation (2), the same result is trivially true for mass and chemical composition: if liquids are chemically isolated from the solids, the velocity of liquid in the isolated melt reservoir

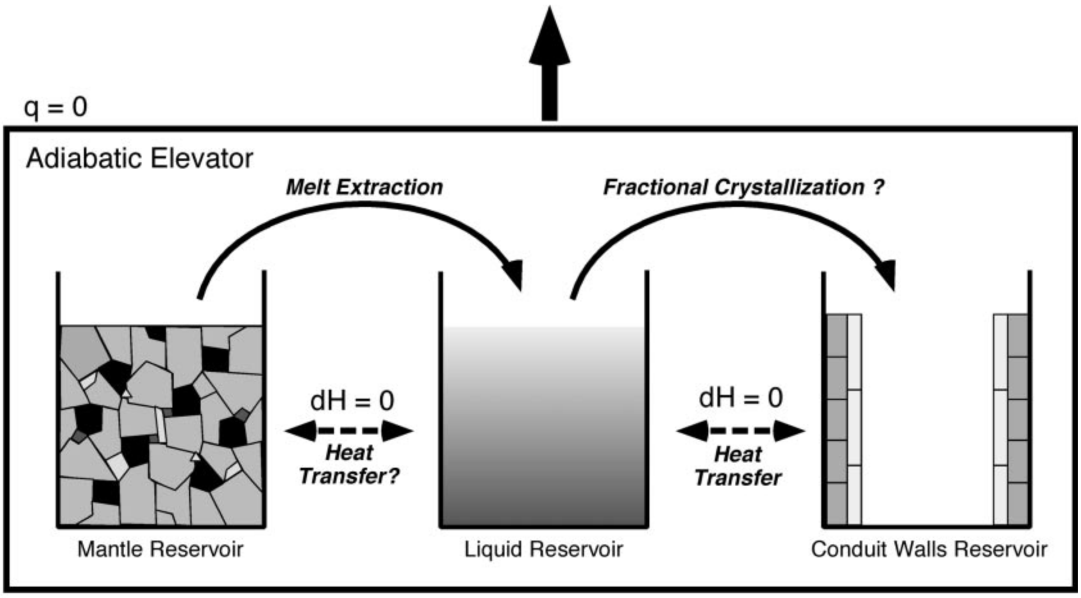

Fig. 1. Schematic drawing representing the calculation of thermal equilibrium between ascending mantle, the liquid reservoir containing accumulated fractional melts, and possibly a reservoir of crystals fractionated from the melt. The system is enclosed in an insulating box through which no heat flows. The reservoirs move together, but this represents any steady one-dimensional solution in which relative flow between mantle and liquid takes place, as long as there is either no thermal interaction or perfect thermal equilibration (see text). In each incremental step, the pressure is lowered reversibly and each reservoir moves up isentropically. Except in the BATCH calculation, any melt that forms in the mantle reservoir is extracted to the liquid reservoir and mixed isenthalpically with its previous contents. Then, optionally, the mantle and liquid reservoirs may be brought to the same temperature at constant total enthalpy (called 'thermal equilibration' in the text). Furthermore, if the liquid in the liquid reservoir crosses below its liquidus, it may either be kept as a metastable liquid or allowed to fractionally crystallize in which case the crystals are removed to the third chemically isolated reservoir, the 'conduit walls'. The conduit walls continue to participate in the thermal equilibrium; that is, the total enthalpy of the three reservoirs is held constant except during the isentropic vertical motion step.

after separation from the solids can have no effect on the composition of the solids and conversely the flux of each component in the accumulated melt is fixed by the mass of that component contributed to the melt at deeper levels and is independent of relative melt velocity.

In each of the two end-member cases considered below, the entropy fluxes and extents of melting are independent of relative melt and matrix velocity as well. For the case of no thermal interaction, this result is again trivial because the entropy flux in the liquid reservoir at any level is determined by the sum of contributed entropy at deeper levels, unaffected by any further interaction with the solid reservoir. For the case of perfect thermal equilibration, the entropy flux in the liquid reservoir is affected by its temperature at each pressure (i.e. entropy flux is given by mass flux times specific entropy, which is a function of composition, temperature, and pressure; as mass flux and composition are independent of relative velocity, melt separation can only affect entropy flux at any pressure via temperature changes), but liquid and solid reservoirs have a common temperature in this limiting case no matter what their relative velocities. Clearly, intermediate cases with partial thermal equilibration between the liquid and solid reservoirs will have outcomes that are dependent on the relative rates of upward flow and thermal diffusion. Considering only the limiting cases of perfect thermal isolation and perfect thermal equilibration, however, one need only calculate the situation where the residual mantle and the chemically isolated accumulated fractional melt travel together at the same velocity. The same results will hold for any permeability function and separation velocity, so long as perfect thermal equilibration remains physically reasonable. In contrast, as discussed above, the gravitational potential release term is not independent of relative melt velocity, but there is a well-defined maximum effect produced in the case of infinite permeability.

Method

The numerical experiment used to evaluate the various impacts of melt migration on melt production according to MELTS is illustrated in schematic form in Fig. 1. The calculations proceed in a series of discrete steps. A parcel of mantle material is isentropically decompressed by 5 MPa at equilibrium until a small increment of melt ($\sim$0·001% by volume) is present. The melt is then

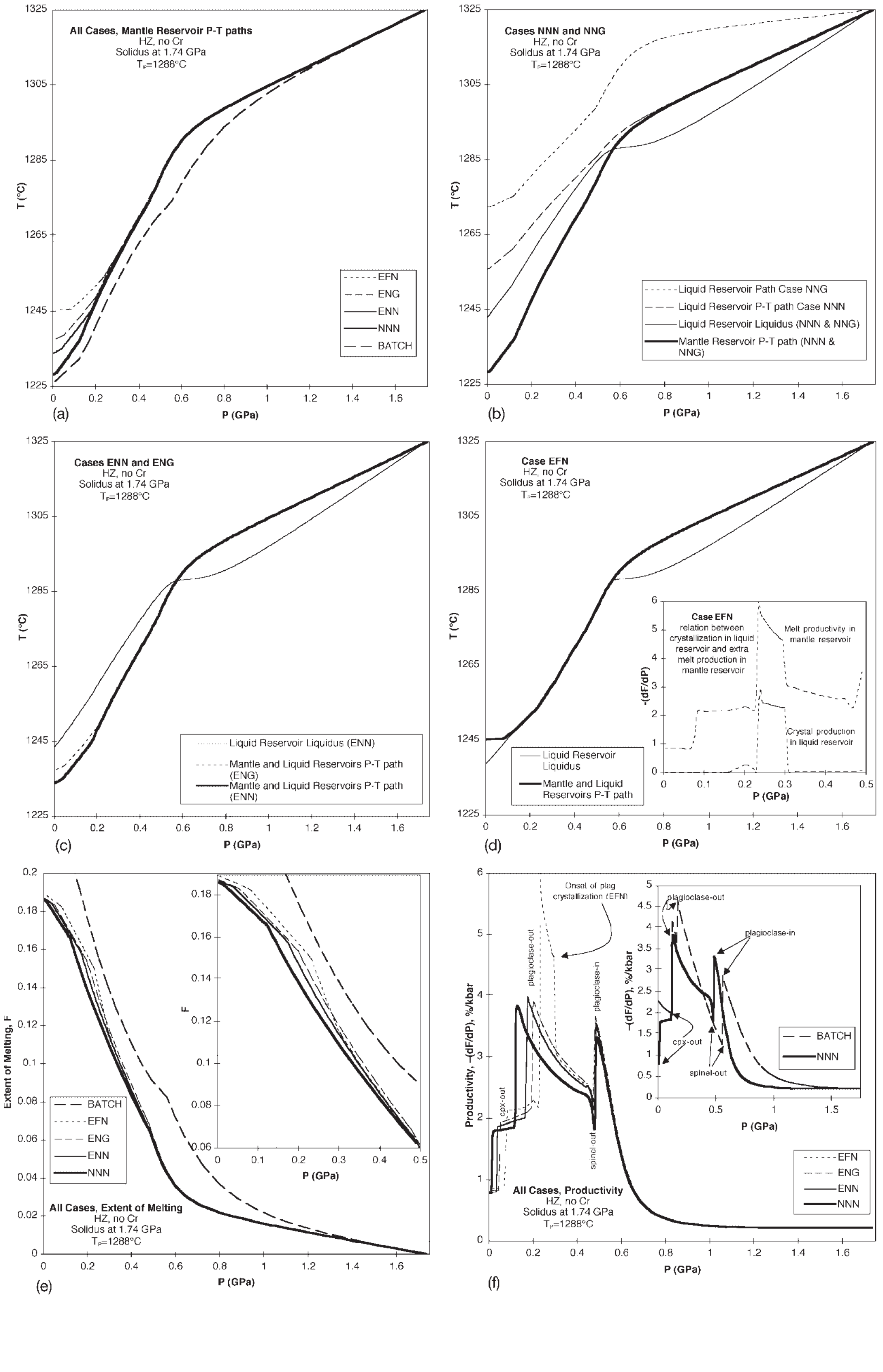
All Cases, Mantle Reservoir P-T paths
HZ, no Cr
Solidus at 1.74 GPa
T (°C)
P (GPa)
EFN
ENG
ENN
NNN
BATCH
(a)
Cases NNN and NNG
Liquid Reservoir Path Case NNG
Liquid Reservoir P-T path Case NNN
Liquid Reservoir Liquidus (NNN & NNG)
Mantle Reservoir P-T path (NNN & NNG)
(b)
Cases ENN and ENG
Liquid Reservoir Liquidus (ENN)
Mantle and Liquid Reservoirs P-T path (ENG)
Mantle and Liquid Reservoirs P-T path (ENN)
(c)
Case EFN
relation between crystallization in liquid reservoir and extra melt production in mantle reservoir
Melt productivity in mantle reservoir
Crystal production in liquid reservoir
-(dF/dP)
Liquid Reservoir Liquidus
Mantle and Liquid Reservoirs P-T path
(d)
All Cases, Extent of Melting
Extent of Melting, F
F
(e)
All Cases, Productivity
Productivity, -(dF/dP), %/kbar
Onset of plag crystallization (EFN)
plagioclase-out
plagioclase-in
cpx-out
spinel-out
-(dF/dP), %/kbar
(f)

extracted at constant pressure into a separate reservoir that is initially empty; this segregation does not affect the specific entropy of either liquid or residue. Thus the 'mantle' reservoir and the accumulated fractional melt ('liquid', for brevity) reservoir begin at the same temperature, and the first increment of melt in the liquid reservoir begins on its liquidus. Next, both the mantle and the liquid reservoirs are moved 5 MPa lower in pressure isentropically (each on its own separate adiabat) and the mantle reservoir again undergoes a small increment of melting. Again the melt is extracted, and this time and henceforth it is mixed isenthalpically with the previously accumulated liquids.

Now, in general, at this point the mantle and liquid reservoirs will be at different temperatures. Here several choices are made and the resulting case is named by a three-letter code. The first letter describes whether the mantle and liquid reservoirs are now equilibrated to the same temperature (Exx) or left at their separate temperatures (Nxx). The second letter describes whether the liquid reservoir is maintained as a (possibly metastable) liquid (xNx), or permitted to undergo fractional (xFx) crystallization. The third letter indicates whether the maximum limiting gravity term [equation (7)] is added to the entropy of the liquid reservoir (xxG) or not (xxN). The cases considered for comparison below are:

NNN (no thermal equilibration, no crystallization, no gravity);

NNG (no thermal equilibration, no crystallization, gravity added);

ENN (complete thermal equilibration, no crystallization, no gravity);

ENG (complete thermal equilibration, no crystallization, gravity added);

EFN (complete thermal equilibration, fractional crystallization, no gravity).

All are compared with the equilibrium porous flow or BATCH case, which is calculated according to the method of Asimow & Stolper (1999).

For case NNN, nothing further happens before the two reservoirs are again decompressed on their separate adiabats. In the NNG case, the gravity term is taken to describe dissipation in the liquid and simply makes the liquid hotter, but does not in this case feed back into melting. This case is shown only so that the magnitude of the excess entropy as a result of gravity can be seen in simple thermal terms rather than filtered through the rather complex melt production function. For all cases with thermal equilibration, the mantle and liquid reservoirs are now brought to the same temperature at constant total enthalpy, an irreversible step associated with a small increase in entropy. During this step, the mantle reservoir is kept at equilibrium; that is, because it is right at its solidus following the extraction of melt, when heated by interaction with the liquid reservoir it produces some additional melt (which is for the moment left in the mantle reservoir).

The next choice is whether to allow fractional crystallization in the liquid reservoir. For cases ENN and ENG, the liquid reservoir is maintained as a (possibly metastable) liquid, regardless of whether it crosses its liquidus. For the EFN case, if the liquid reservoir is below its liquidus, it is permitted to crystallize solid phases. This crystallization takes place isenthalpically, and the latent heat of crystallization liberated enters into the total enthalpy budget of the isobaric thermal equilibration step, resulting in a further rise in temperature (and increase in entropy) of the mantle and liquid reservoirs and additional melting in the mantle reservoir. As solids form in the liquid reservoir they are extracted to a third chemically isolated reservoir, which can be thought of as the 'conduit walls' in a real mantle plumbing system. The conduit-walls reservoir participates

Fig. 2. Illustration of the effects of chemical isolation, thermal equilibration between accumulated fractional melt and the mantle, crystallization of the melt, and entropy production as a result of gravity and friction in a MELTS calculation of peridotite melting. The various cases (BATCH, NNN, NNG, ENN, ENG, and EFN) are explained in the text. In this example the potential temperature is 1288°C and all cases begin melting at 1·74 GPa. (a) The P–T paths of the mantle reservoir in five cases are compared (skipping NNG); for all cases except NNN this is also the path of the liquid reservoir. The four fractional cases differ significantly only below 0·3 GPa. (b) Case NNN: fractional melting, no thermal equilibration, no crystallization of liquid reservoir, no gravity term. The P–T paths of the mantle and liquid reservoirs are plotted together with the locus of liquidus temperatures of the liquid reservoir at each pressure. The path of the liquid when gravitational energy is dissipated in this reservoir (case NNG) is also shown. (c) Cases ENN and ENG: liquid and residual reservoirs are brought to equal temperature at each pressure, crystallization is not allowed in the liquid reservoir, gravity term excluded and included. The liquid is metastable below 0·6 GPa but is not permitted to crystallize. Gravity causes a small amount of heating visible at the end of the path. (d) Case EFN; the amount of crystallization that occurs is generally related to the undercooling of the liquid reservoir with respect to the liquidus curve shown in (c), but in the case of fractional crystallization the liquidus and the liquid reservoir temperature are coincident so long as crystallization is taking place. The inset shows the coupling between mass crystallized per unit pressure from the liquid reservoir and melt productivity in the mantle reservoir. (e) Melt fraction, F, vs P for the five distinct cases. The differences among the fractional cases are small, especially at low pressure where all the cases have exhausted residual plagioclase and clinopyroxene. The inset shows an enlargement of the low-pressure part of the plot. (f) Melt productivity, $-(dF/dP)$, vs P for the four fractional cases; the BATCH case is shown only in the inset because it crosses the other curves in ways that obscure the differences between them. Here the differences among fractional cases are clearly visible. Each curve shows three drops in productivity, at the spinel–plagioclase transition (0·5–0·6 GPa), plagioclase-out (0·15–0·25 GPa), and cpx-out (<0·1 GPa). The higher-productivity cases experience each productivity drop at higher pressure. The large productivity spike in the crystallization cases is due to the crystallization of plagioclase + olivine from the liquid reservoir, as seen in the inset to (d).

in the thermal equilibrium; that is, its enthalpy is considered in maintaining constant total enthalpy during the thermal equilibration step and it stays at the same temperature as the mantle and liquid reservoirs (this reservoir is far below its solidus and does not melt during the thermal equilibration step in any of the calculations performed here; furthermore, the various solid phases in this reservoir do not react with one another). At the end of the isenthalpic equilibration step, the individual entropies of all three reservoirs at the new temperature are calculated, and these are used as references for the next isentropic decompression of each reservoir on its own adiabat. This calculation is repeated until the pressure reaches the base of the crust (<250 MPa for all cases considered). The calculation is continued all the way to low pressure to observe the range of possible behaviors in the plagioclase peridotite stability field, but this is not meant to imply that adiabatic melting (or indeed any melting) continues to such a low pressure in any real environment. Much of the interesting behavior noted below for low initial potential temperatures of the mantle reservoir occurs entirely at pressures that in reality are in the conductive lithosphere. The conclusions about mantle reservoirs at 'normal' temperatures (i.e. temperature sufficient to exhaust cpx at or before the minimum pressure of melting), however, are not sensitive to the pressure of final melting in these calculations.

A representative calculation

P–T paths for the various cases are shown in Fig. 2a–d for the Cr-free analog of the Hart & Zindler (1986) primitive upper-mantle source composition on the adiabat that intersects its solidus at 1·74 GPa. The potential temperature according to MELTS is 1288°C. The corresponding values of extent of melting, F, and its derivative, $-(dF/dP)$, the melt productivity, are plotted against P in Fig. 2e and f. This representative calculation is performed for a rather cold mantle (i.e. cold enough for a fractionally melting peridotite to encounter the plagioclase lherzolite stability field at low pressure). Although this potential temperature results in only 2·7 km of crust for case NNN and 3·6 km of crust for batch melting, I explore it in detail because it expresses a richer spectrum of behavior than hotter adiabats, especially in case EFN. After discussion of these results, the next subsection will show the range of behaviors that results from a range of potential temperatures.

Cases NNN and NNG (no thermal equilibrium, no crystallization, without and with gravity)

The shape of the P–T path for the mantle reservoir in the 'no equilibration' case (bold continuous curve in Fig. 2b) is controlled by the melt productivity of incrementally isentropic fractional fusion; the sources of variations in productivity and hence in P–T slope were explored by Asimow *et al.* (1997). For this relatively low potential temperature, the fractional melting path encounters the spinel-to-plagioclase lherzolite transition at 0·5 GPa. It then exhausts plagioclase at 0·15 GPa and cpx just before reaching 1 bar; these changes in the residual phase assemblage are all visible as drops in productivity in Fig. 2f. The P–T path of the liquid reservoir differs from a simple liquid adiabat because liquids at the temperature of the mantle reservoir are added to it at each step; thus its shape (the light long-dashed curve in Fig. 2b) is related to the shape of the mantle P–T path. Nevertheless, the liquid reservoir still evolves to a higher temperature than the mantle reservoir, as it follows an all-liquid adiabatic path during each decompression step. In this NNN case, the liquid reaches 1 bar at a temperature 27 K higher than the mantle; this temperature excess represents the excess entropy advected by the melt, which can be recovered by the mantle when the mantle and melt are thermally equilibrated in the cases discussed below. In case NNG, the gravitational source term does not feed back into the mantle reservoir as the gravitational energy is assumed to be dissipated entirely in the melt reservoir, and the resulting heating of the liquid reservoir results in a 1 bar temperature of this reservoir (dotted curve in Fig. 2b) 44 K higher than the mantle reservoir. This indicates that the magnitude of excess entropies (seen in this case as excess temperatures) available from thermal equilibration (27 K) and from the gravitational source term (another 17 K) are comparable.

The calculated liquidus temperature of the liquid reservoir is also shown at each pressure in Fig. 2b (fine continuous curve). It should be noted that this is not the liquidus curve of any particular partial melt of the peridotite, as the chemical composition of the liquid reservoir changes each time a new increment of melt is added. Nevertheless, the locus of liquidus temperatures shows some important systematics. In the initial stages of melting, when the slope of the P–T path of the mantle reservoir is low (reflecting low productivity; Asimow *et al.*, 1997), the liquidus drops off in temperature more quickly than the P–T path of the mantle reservoir. Hence, although this may seem counterintuitive and contrary to the behavior assumed by Kinzler *et al.* (1993), cooling of accumulated fractional liquids to the ambient temperature of the mantle does not necessarily result in crystallization (see case EFN below). At higher extents of melting, however, the mantle P–T path is steeper (the result of increased melt productivity requiring larger absorption of latent heat and hence larger drops in T on the P–T path of the mantle reservoir) and crosses the liquidus of the melt in the liquid reservoir near the pressure at which 5% total melting has taken place. At this level, crystallization from accumulated fractional liquids cooled to the temperature of the ambient mantle is possible. Although the detailed relationships between F, $-\mathrm{d}F/\mathrm{d}P$, and these temperature differences depend on uncertain aspects of the MELTS model, the relationship between $\mathrm{d}T/\mathrm{d}P$ of the mantle path and productivity is well constrained, so it can be said with somewhat greater certainty that this crossover occurs near a productivity of 1%/kbar. It should be noted that the constraint that fractional crystallization of accumulated fractional melts is thermally prohibited until the system exceeds a certain melt productivity limits the range of problems that can be solved by appeal to such deep crystallization. The suggestion of Kinzler *et al.* (1993) concerning excess olivine in abyssal peridotites (relative to that expected from fractional melting of fertile lherzolite) is still valid in principle, but will need to be reconsidered quantitatively with better constraints on the thermal environment. It should be noted also that for potential temperatures lower than 1270°C (not plotted in these figures), the liquidus of the liquid reservoir compositions crosses the liquid reservoir P–T path in the NNN case, and hence crystallization could occur from the accumulated fractional liquids even without any cooling by the surrounding mantle. This behavior has been observed only in the plagioclase lherzolite stability field.

Cases ENN and ENG (thermal equilibrium, no crystallization, without and with gravity)

The case of thermal equilibration with no crystallization is shown in Fig. 2c. The accumulated fractional liquid and mantle reservoirs follow coincident P–T paths. Figure 2a compares the mantle reservoir P–T paths from the various cases (which is also the liquid reservoir P–T path for cases BATCH, ENN, ENG, and EFN); the mantle reservoir in the ENN case reaches 1 bar at a temperature 5·5 K higher than the mantle reservoir in the NNN case, and conversely the liquid reservoir forced to the same temperature as the mantle reservoir in the ENN case reaches 1 bar at a temperature 22 K lower than the liquid reservoir in the NNN case. This partitioning of the 27 K of available temperature difference between the reservoirs in case NNN into a $\sim$4:1 ratio of heating of the residue and cooling of the liquid is similar to the mass ratio of the two reservoirs at the final extent of melting of $\sim$20%. The addition of the limiting gravity term to case ENG causes the mantle and liquid reservoirs to reach 1 bar at a temperature a further 3·5 K higher than case ENN, showing again that the effect of gravity is comparable with, but smaller than, the effect of thermal equilibration.

The liquids in cases ENN and ENG are metastable from 0·6 GPa to 1 bar, the range where they are below their liquidus (Fig. 2c; the liquidus paths for ENN and ENG are very similar), but crystallization is prohibited in this case. Figure 2f shows that thermal equilibration in the ENN case causes melting to be up to 18% more productive than the NNN case in the 0·17–0·5 GPa pressure range, and as a result the ENN case exhausts plagioclase from the residue earlier (and is then less productive in the pressure range 0·12–0·17 GPa, where case NNN is still melting plagioclase lherzolite). The ENN case also exhausts cpx earlier than case NNN (at 0·04 GPa rather than 0·02 GPa). The net result of these productivity changes and phase exhaustions, as shown in Fig. 2e, is that the final melt fraction achieved at 1 bar (F_{max}) is almost identical in the two cases, although the mean pressure of melt production (not plotted) is slightly higher for case ENN (by 0·015 GPa, or 6%).

As expected from the relative magnitudes of liquid temperature excess (in the comparison of cases NNG and NNN above) and from the temperature difference at 1 bar between cases ENG and ENN, the addition of the gravity term in case ENG increases productivity by about half again as much as the thermal equilibration term (e.g. by 23% relative to NNN just before plagioclase exhaustion at 0·2 GPa, where ENN productivity is 15% greater than NNN). This causes similar increases in the depths of the phase exhaustion points and in the mean pressure of melting.

Case EFN (thermal equilibrium, fractional crystallization, no gravity)

The P–T path of mantle and liquid reservoirs and the liquid reservoir liquidus for the EFN case are shown in Fig. 2d. It should be noted that the liquidus of the liquid reservoir is restricted to be equal to the temperature of the liquid reservoir whenever fractional crystallization occurs (i.e. between 0·6 and 0·2 GPa). Crystallization of olivine begins after the liquid reservoir and mantle reservoir P–T paths cross the liquidus temperature of the liquid reservoir at $\sim$0·6 GPa for this potential temperature, later to be joined by plagioclase crystallization at 0·3 GPa. Crystallization continues so long as the liquid reservoir P–T path remains steeper than its liquidus would be in the absence of crystallization. Once crystallization begins, in all the cases examined it proceeds until a phase is exhausted from the residue in the mantle reservoir; when this occurs, there is a drop in productivity, a smaller slope of the mantle reservoir (and liquid reservoir) P–T path, and hence no further crystallization (we have also calculated the equilibrium crystallization problem, where resorption occurs at low pressure; the results are distinct from EFN only for very low potential temperatures).

As explained above, when crystallization occurs in the liquid reservoir, it has an effect on productivity, and Fig. 2f and the inset to Fig. 2d demonstrate that this effect can be significant, particularly when the liquid reservoir is multiply saturated and experiences a large amount of crystallization per unit temperature drop. The effect is a consequence of the imposed conservation of enthalpy at each pressure: the enthalpy recovered by crystallizing in the liquid reservoir goes into melting the mantle reservoir. The total liquid mass in the two reservoirs may increase, remain constant, or decrease during this process, depending on the relationship between the enthalpy of crystallization of the assemblage crystallizing from the liquid reservoir, the enthalpy of fusion of the mantle reservoir, and the heat capacity of the system. The composition of the liquid remaining in the liquid reservoir can also be shifted somewhat by this crystallization; the direction of this compositional shift depends on what minerals are crystallizing (olivine or olivine + plagioclase in all the cases explored). The result is an unusual form of melt–mantle reaction in which thermal exchanges cause modification of both melt and residue chemistry despite lack of direct chemical interaction.

The large increase in productivity shown in Fig. 2f for cases EFN begins near 0·3 GPa, where plagioclase joins olivine in the fractionating assemblage and the change in crystal mass with pressure jumps to $\sim$2%/kbar (referenced to the original source mass; i.e. in units comparable with melt productivity). In contrast, olivine crystallization beginning at 0·6 GPa has only a small effect (compare with case ENN between 0·3 and 0·6 GPa in Fig. 2f), reflecting the small amounts of olivine crystallization for a given temperature drop when olivine is the only crystallizing phase (at the onset of plagioclase saturation, only 1% of the liquid has crystallized). The productivity spike ends at 0·24 GPa when the residue in the mantle reservoir exhausts plagioclase, at which point a total of $\sim$15% of the liquid (i.e. $\sim$2% of the entire system) has crystallized. Crystallization also stops at this point because productive melting of the mantle reservoir is no longer forcing the liquid reservoir to cool with respect to its liquidus; consequently, the cases with crystallization cease at this point to be more productive than the other cases. The slopes of the liquidus paths in these calculations are such that a large productivity (>2%/kbar) in the mantle reservoir is a prerequisite for crystallization in the liquid reservoir, which leads in turn to higher productivity in the source. The magnitude of the excess productivity as a result of crystallization then depends principally on how large the isentropic productivity is (i.e. how much undercooling it drives) and on the fractionating assemblage (i.e. how much crystallization and how much latent enthalpy release there is per degree of undercooling, relative to the enthalpy of fusion of the mantle assemblage).

Although the increase in productivity over case ENN between 0·2 and 0·3 GPa in the cases with crystallization (EFN) is large, the increase in maximum F achieved at 1 bar is, as described above for the other cases, extremely small because of the limitations imposed by phase exhaustion (Fig. 2e). Although the F curves for the various cases are visibly separated in the range 0·1–0·5 GPa, the kinks at the exhaustion of plagioclase from the residue in each case 'refract' this visible difference to a very small difference at pressures below the kink. There is a second kink (see inset to Fig. 2e) on each curve at the exhaustion of cpx from the residue, which further limits the differences in F along the various curves at pressures lower than that of the kink. Even though thermal equilibration and crystallization in the liquid reservoir add entropy to the mantle, its extent of melting is limited by the low productivity that follows phase exhaustion; that is, the low productivity of fractional melting of harzburgite prevents the added entropy from increasing the final melt fraction very much in this example, which happens to exhaust cpx in case NNN just before reaching 1 bar. Calculations in which exhaustion of cpx and/or plagioclase do not limit total melting to a value near that for case NNN can be seen below in the section that considers the impact of variations in potential temperature on these results.

BATCH case

It can readily be seen from Fig. 2a, e and f that the BATCH path follows the coldest P–T path and yields the highest extent of melting and melt productivity. Because this path is strictly isentropic, these results are all coupled; that is, the BATCH path evolves to the lowest temperature because it produces the most melt. The instantaneous bulk composition of the mantle reservoir is unchanging over the course of the batch melting process, but it changes continuously and differently for each of the various fractional melting cases shown in Fig. 2. Consequently, the P–T–F paths differ in each of these cases and it does not violate any rules to have higher melt fraction at lower temperature. However, among the various fractional cases (NNN, ENN, ENG, EFN), the opposite relation exists between temperature and extent of melting (i.e. higher temperatures correspond to higher melt fractions), as the differences among these cases reflect entropy production in the melting system rather than different distributions of the same total entropy between latent heat and temperature changes.

The tendency for equilibrium melting to be generally more productive than batch melting in multicomponent systems is well known (Presnall, 1969), and it is sometimes attributed to the progressive rise in the solidus temperature of the residue as more melt is extracted from the system (e.g. Morgan, 2001). Previous studies have explored exceptions or qualifications to this tendency in simple and complex systems, including the equality of productivity for batch and fractional melting right at the solidus, the tendency in certain cases for the productivity of fractional melting to overtake that of batch melting at high melt fraction, and the importance of whether productivity is defined relative to the initial mass of the system or to the continuously decreasing mass of a source undergoing fractional melting (Asimow *et al.*, 1995, 1997; Hirschmann *et al.*, 1999*a*). We have also shown that MELTS models of peridotite partial melting predict that one of the most significant differences between batch and fractional melting (the NNN case) is that although productivity drops discontinuously (from a peak of perhaps 3%/kbar) upon exhaustion of clinopyroxene in both cases, it remains low ($\leq$1%/kbar) for the fractional melting case but recovers within $\sim$0·2 GPa back to 2%/kbar or more for batch melting (Asimow *et al.*, 1997). This is an important issue here because the low productivity of fractional melting of harzburgite limits the amount of extra melting that can be produced by any of the sources of excess entropy in any of the fractional cases discussed above.

The key point is that the suppression of melting by the process of fractional fusion (i.e. by the extraction and chemical isolation of the most fusible components of the system, particularly upon the exhaustion of a residual phase) is a much larger effect than any of the thermal or irreversible consequences of melt migration under consideration and hence that if melt migration leads to chemical disequilibrium then for mantle compositions it will produce less melt and thinner crust than the closed-system case. Only if melt migration proceeds in chemical (and thermal) equilibrium can the gravity source term cause it to be more productive than the closed-system case, and even this is a small effect ($\leq$100 m of extra crust).

The range of possible behaviors

The magnitudes of the effects on productivity of thermal equilibration and crystallization of the liquid reservoir in these calculations vary with potential temperature. The productivity of decompression melting at any given pressure varies with potential temperature, as do the occurrence and effects of subsolidus phase changes and the extents of melting needed to exhaust garnet, spinel, plagioclase, and cpx from the residue. All these effects control the slope of the *P–T* path of the mantle and liquid reservoirs and hence the relationship of the liquid reservoir path to its liquidus and the occurrence and amount of crystallization in the liquid reservoir. Phenomena related to residual plagioclase and crystallization of plagioclase from the liquid reservoir are restricted to low potential temperatures.

The overall effects of thermal equilibration and crystallization are shown as functions of potential temperature in Fig. 3. Figure 3a shows the maximum F (F_{max}, defined as the mass fraction of the mantle reservoir removed as melt into the liquid reservoir; in cases in which crystallization occurs in the liquid reservoir, this can be larger than the amount of melt that can be erupted or intruded into the crust) achieved at the base of the crust in each case. The key result is that sources of excess entropy in the fractional cases (that is, thermal equilibration, crystallization from the liquid, and/or gravity) have negligible effects on the maximum melt fraction achieved for all those adiabats with potential temperature above 1300°C, but the difference between equilibrium and fractional processes persists and continues to increase with rise in potential temperature. As discussed above, the similarity of F_{max}, for all the fractional fusion cases with potential temperature above $\sim$1300°C is the result of the effective limitation of fractional melting by the exhaustion of clinopyroxene. Hence if the calculations shown in Fig. 3 were redone with melting stopping at greater depth than the base of the oceanic crust (e.g. as a result of conductive cooling beneath the base of the crust), the maximum potential temperature for which sources of excess entropy could have significant effects on F_{max} would rise from $\sim$1300°C to approximately the potential temperature at which cpx would be exhausted for the NNN case at the pressure at which melting stops; this is also the approximate position of the break in slope of the F_{max} vs potential temperature curve for the NNN case (Fig. 3a).

Although fractional melting continues beyond the exhaustion of cpx, the isentropic (and isobaric) productivity is very low, and the amount of entropy that would need to be added to the mantle by thermal equilibration or crystallization to produce significant melting is correspondingly large. Therefore, an alternative indicator of the differences between the cases considered is shown in Fig. 3b by the pressure of exhaustion of cpx from the residue, which is changed in the various fractional cases by the thermal, gravity, and crystallization effects by up to $\sim$0·1 GPa. A potential temperature of 1300°C is the maximum at which cpx remains in the residue in case NNN at the base of the crust (and is thus the highest potential temperature at which significant differences in F_{max} occur as a result of the thermal and irreversible effects considered here), explaining, as described above, why these sources of excess entropy have minimal influence on F_{max} at potential temperatures above 1300°C in Fig. 3a. Figure 3b also shows that there is a small increase in the pressure of cpx-out associated with thermal equilibration for all potential temperatures, reflecting the increases in degree of melting produced by thermal equilibration at all depths, which in turn leads to deeper achievement of the degree of melting required to exhaust cpx. This change in pressure of cpx-out as a result of thermal equilibration alone is essentially independent of potential temperature. Figure 3b shows again that the

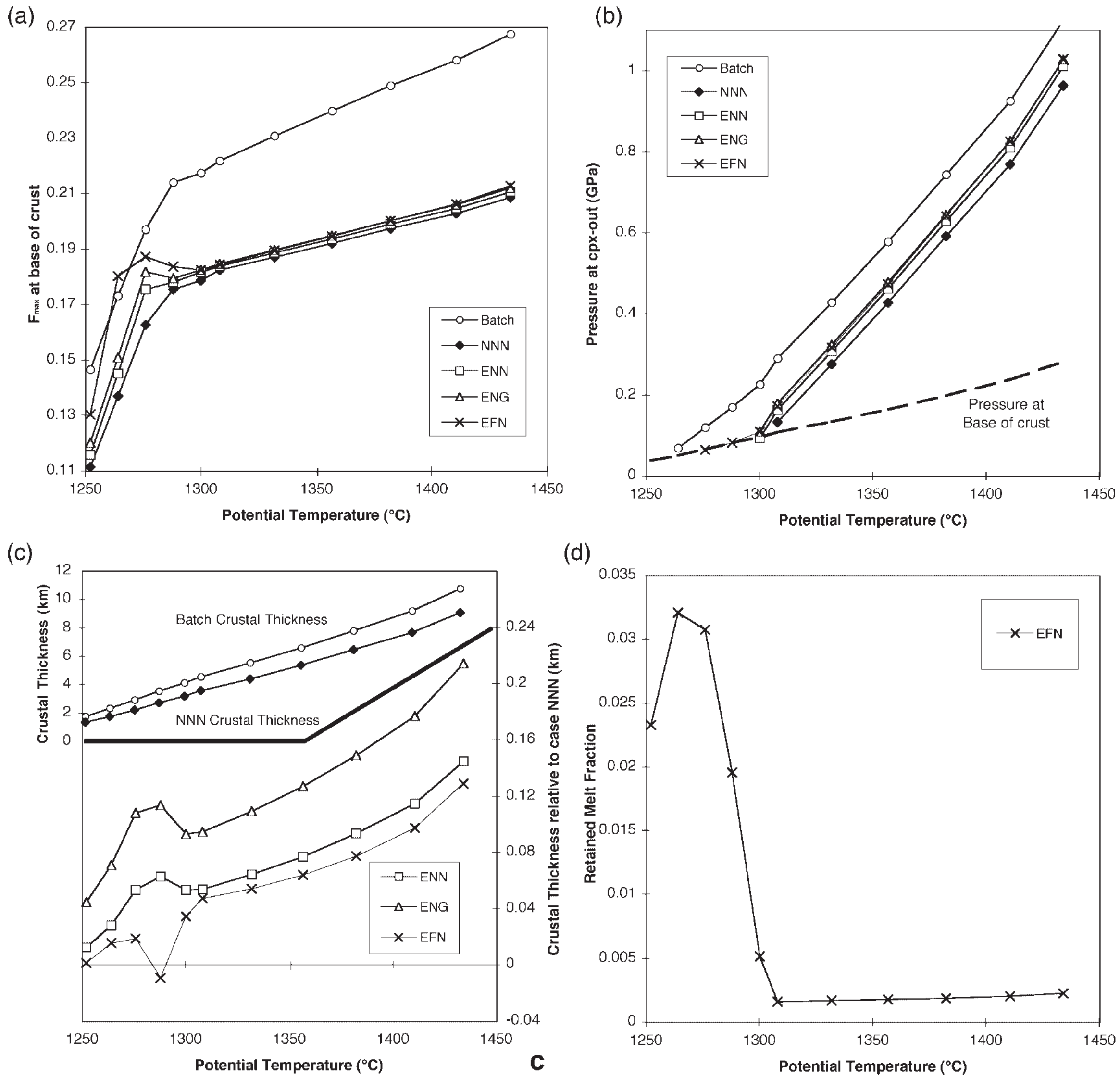

Fig. 3. The net effects of the various cases considered for melting regimes with a wide range in potential temperature (T_P, a monotonic function of solidus intersection pressure and of the specific entropy of the material entering the base of the melting column). (See text for explanation of cases BATCH, NNN, ENN, ENG, and EFN.) (a) F_{max}, the melt fraction by mass reached at the base of the crust, measured by the total extracted from the mantle residue, whether or not it all reaches the crust. (b) The pressure at which clinopyroxene is exhausted from the residue; the pressure at the base of the crust for case NNN is indicated for comparison. (c) On the left-hand scale, the crustal thickness for cases BATCH and NNN from a two-dimensional passive flow melting regime [using the formalism of Klein & Langmuir (1987)], measured by the bulk melt fraction remaining as liquid after any crystallization in the mantle. The relative extra crustal thickness compared with case NNN for the other fractional cases is also shown (right-hand scale). (d) The mass retained in the mantle as solids for case EFN, expressed in terms of equivalent missing melt fraction.

principal effect of adding thermal interaction and/or gravity to the fractional melting columns is to cause a drop, by ~40°C in the EFN case (from 1300°C to 1260°C), in the potential temperature needed to exhaust cpx from the residue in the shallowest part of the mantle section.

Figure 3c shows the absolute crustal thickness generated in cases BATCH and NNN assuming simple passive flow geometry (Forsyth, 1992); the range of potential temperatures explored yields crustal columns from 1·8 to 10·8 km thick by BATCH melting and from 1·3 to 9·1 km thick for case NNN. The difference between these extremes increases from 400 m to 1·7 km as potential temperature rises from 1250 to 1430°C. Figure 3c also shows the differential crustal thickness for the various fractional cases compared with the reference case NNN. The maximum excess crustal production, for case ENG at $T_P = 1430$°C, is $\sim$220 m, added to the 9 km of crust generated by case NNN. Generally the extra crustal thickness is negligible, and the effects of adding both the thermal energy from hot migrating liquids and the maximum dissipation as a result of friction and melt migration in a gravity field do not nearly approach the crustal thickness lost in the fractional melting cases relative to the batch melting case. A further complication arises from crystallization of the liquid reservoir in the mantle, which would prevent some of the melt extracted from the residue from reaching the crust because crystals are extracted from the liquids when they are still in the mantle (e.g. plated onto conduit walls). Figure 3d shows the mass fraction of the system that is retained in the conduit-walls reservoir in case EFN (relative to the original source mass), which can be as much as 3%, and is therefore significant compared with F_{max} values near 18%. Consequently, supposing that only liquid in the liquid reservoir at the end of these calculations (at the base of the crust) is available to become part of the crust, Fig. 3c shows that case EFN can actually generate less crust than case NNN within a narrow range of potential temperature where rapid crystallization of plagioclase from the liquid is not balanced by productive melting of plagioclase peridotite.

Figure 3 demonstrates that changes in crustal thickness and residual mineralogy resulting from thermal interactions below the conductive boundary layer are negligible for a model in which melting continues to the base of the crust except for extremely cold regions of the mantle where this crust is very thin. At potential temperatures above 1300°C, negligible crystallization occurs (Fig. 3d) because the liquid reservoir path does not cross the liquidus or does so only for a small pressure range, with a small amount of undercooling and very minor olivine crystallization. Consequently, for such potential temperatures, the effects on liquid chemistry and residue mineralogy of fractionation along the adiabat are negligible in the context of MELTS calculations (contrary to Kinzler *et al.*, 1993). It should be noted that, according to MELTS, a potential temperature of 1300°C generates, by passive flow and fractional fusion, <4 km of oceanic crust, so nearly the entire ridge system (with normal crustal thickness exceeding 6 km) should be drawing on mantle hot enough that sublithospheric crystallization is negligible. For potential temperature lower than 1300°C, the principal effects of thermal interactions are to increase the maximum melt fraction, but to values no higher than the melt fraction needed to achieve cpx exhaustion, which is usually not much higher than the melt fractions generated in the absence of thermal interactions. Significant changes in liquid chemistry occur only as a result of plagioclase crystallization and enhanced melting of plagioclase peridotite along abnormally cold adiabats at low pressure.

Gravitational–frictional source term as a function of potential temperature

In the example calculation at $T_P = 1288$°C (Fig. 2), the magnitude of the limiting entropy source as a result of gravity and friction was seen to be similar to the entropy source available from thermal equilibration between liquid and solid, but about 50% smaller. This was seen both in the comparison of the temperatures of the liquid reservoirs at 1 bar in cases NNN and NNG (Fig. 2b) and in the comparison of productivity between cases NNN, ENN, and ENG (Fig. 2f). The same approximate similarity of these two quantities holds true across a wide range of potential temperatures. Thus, for a higher potential temperature of 1430°C (melting begins at 3·1 GPa), the excess temperatures of the liquid reservoir above the mantle reservoir at 1 bar in cases NNN and NNG, showing the magnitude of the entropy sources in a simple thermal form, are 32 and 63 degrees. Figure 3c shows that when these entropy sources are allowed to drive melting, in cases ENN and ENG, the additional crustal thickness contributions as a result of thermal equilibration and owing to gravity are comparable within a factor of two across the entire potential temperature range studied, but gravity is the larger contribution at low T_P and thermal equilibration is the larger term at high T_P. However, both entropy sources, gravitational dissipation and thermal interaction with liquid, scale like the integral of $F\mathrm{d}P$, and hence drive only limited extra melting because the upward concavity of $F(P)$ implies that the integral of $F\mathrm{d}P$ remains small over most of the range from the solidus up to a pressure close to cpx-out, after which extra melting is limited by the low productivity of harzburgite melting. Although not plotted in Fig. 3c, the effect of adding the limiting gravity–friction term to the equilibrium porous flow (BATCH) case has also been calculated, and it amounts to at most 120 m of extra crust for the $T_P = 1430$°C case, for which isentropic BATCH melting makes 10·8 km of crust.

Summary of the numerical experiments

The two sources of excess melting as a result of melt migration in oceanic melting regimes recognized by McKenzie (1984) (i.e. thermal equilibration with migrating liquids and gravitational energy release) appear to be comparable with one another in magnitude across a wide range of potential temperatures. However, both are negligible for hot mantle (at least up to the maximum studied, 1430°C, whereas McKenzie considered values up to 1600°C), as the extent of melting in such cases is mostly limited by the drop in productivity of fractional fusion when cpx is exhausted from the residue, an effect that is absent in all the melting formulations considered by McKenzie (1984). For abnormally cold mantle (and high spreading rate, to avoid a conductive cap), if melting continues to shallow levels because the crust is thin, there may be increases as the result of both thermal equilibration and gravity (Fig. 3a and c) relative to the simple fractional melting (i.e. NNN) case of up to $\sim 10\%$ (relative) in F_{max} and ~ 100 m in crustal thickness, and corresponding decreases in the mode of residual cpx in the shallowest residues.

My results differ from the simple calculation shown in fig. 8 of McKenzie (1984), in which additional melting is assumed to accumulate linearly with excess entropy input indefinitely; this results in an increase in crustal thickness as a result of irreversible sources that is negligible at low potential temperature and monotonically increases with rise in potential temperature. Furthermore, in the calculations presented here, there are additional effects owing to the possibility of crystallization from the accumulated fractional liquid. This can cause local increases of >100% in the productivity of melting (e.g. Fig. 2f, between 0·25 and 0·3 GPa) for low potential temperatures, but the balance between liquid gained by extra melting and lost by crystallization prevents large increases in crustal thickness by this mechanism.

Although I have not introduced any new physics into the evaluation of the gravity term, the estimate of its magnitude is smaller (by roughly a factor of two) than that of McKenzie (1984) whether compared with his calculations using adiabats with equal potential temperature, adiabats with equal pressure of initial melting, or adiabats that would reach the same F_{max} in the reference case NNN. This is a consequence of the strongly increasing productivity function during progressive decompression melting in MELTS calculations. As mentioned above, the total entropy source owing to gravity is roughly proportional to the integral of $F\mathrm{d}P$. Clearly, for the same F_{max} and the same pressure range of melting, the area under the $F(P)$ curve is much smaller for a strongly concave-up curve than for a linear or concave-down curve (compare the curves in Fig. 2e with the area under a straight line from $F = 0$ at 1·7 GPa to $F = F_{max}$ at 1 bar). The same is true of the MELTS estimates of the effect of thermal equilibration when compared with constant or decreasing-productivity models. Because much of the liquid in a MELTS model of polybaric melting is produced at relatively shallow levels in the melting regime, much of the liquid does not ascend very far along a liquid adiabat, and so less excess entropy is available. In a rough sense, the weighted sum over all increments of melt of the distance that each increment of liquid ascends after being separated from the mantle residue governs the magnitude of the excess entropy that can be recovered through thermal equilibration with the liquid. This quantity, like the magnitude of the gravity term, also scales with the integral of $F\mathrm{d}P$, and hence is smaller in the MELTS model than in simple linear estimates because of the increasing productivity.

Finally, McKenzie (1984) compared the sources of irreversibility treated here and the effects of retaining 3% melt in the matrix with the effects of uncertainties in the 'entropy of fusion' [itself a poorly defined quantity in a natural peridotite (Asimow *et al.*, 1997; Hirschmann *et al.*, 1999*b*)] used in his modeling of isentropic melting, and concluded that the possible increase in calculated crustal thickness as a result of irreversible sources and the possible decrease owing to melt retention were each comparable with the effects of uncertainty in the parameters. Although the definition and values of the terms in the entropy budget are much better known in the context of MELTS modeling, the differences among the various fractional cases considered here are also correspondingly much smaller (because of the cpx-out and integral of $F\mathrm{d}P$ effects) and it remains true that the changes in crustal thickness as a result of thermal and irreversible sources in the one-dimensional model are negligible compared with the uncertainties in the model. On the other hand, the retention of melt in the residue (preventing its addition to the crust without needing to crystallize it), which I have not treated here, can still be a fairly large effect. The change in crustal thickness as a result of retention of 3% melt remains of order $(F_B - 3\%)/F_B$, which is 30% or more for all the cases considered.

CONCLUSIONS

The basic conclusion of this work is that the incrementally isentropic model of fractional fusion serves as an excellent approximation to melt production in adiabatically upwelling mantle despite the potential complications associated with melt migration. This result is similar to the conclusion of McKenzie (1984) that decompression melting is approximately isentropic, but accounting for the effects of chemical and thermal disequilibrium and incorporating a self-consistent approach to calculating melt productivity leads to several new conclusions.

(1) The increasing melt productivity with decreasing pressure and increasing melt fraction that results from isentropic or incrementally isentropic upwelling reduces by about a factor of two the magnitude of the irreversible terms relating to thermal interaction between migrating liquid and residue and to gravitational dissipation, compared with a constant productivity model.

(2) At least in one dimension, the most significant possible effect of melt migration on melt production is the likelihood of chemical segregation of liquids and the resulting disequilibrium transport, leading to a major suppression of melting (amounting to ~ 1 km less crustal production for mid-ocean ridge geometry) as a result of the familiar effects of fractional vs equilibrium melting. Of particular note is that, although equilibrium melting remains reasonably productive beyond the exhaustion of clinopyroxene, fractional melting is strongly suppressed.

(3) For normal mantle potential temperatures that reach the exhaustion of clinopyroxene from the residue, all additional sources of heat or entropy result in little additional melting because of the low productivity of harzburgite melting. Hence, for the fractional process the approximation of incrementally isentropic upwelling is reasonably robust even when melt and residue undergo relative motion (neglecting dissipation owing to shear, which may be significant near the ridge axis). Dissipation as a result of compaction of the solid is negligible unless a steep front in extent of melting arises. The gravitational energy release as a result of melt migration and the advection of heat by the melt phase are both small effects.

(4) For normal mantle potential temperatures, the quantity of crystal fractionation that may occur from migrating liquids below the conductive boundary layer is negligible, but adiabats that are cold enough for the liquid to saturate with plagioclase at depth may experience significant modification and drive extensive shallow melting.

ACKNOWLEDGEMENTS

The author wishes most of all to thank Ed Stolper for his unselfish support throughout this project. Thanks also go to Frank Spera and an anonymous reviewer for helpful reviews, and to George Bergantz for editorial handling. Discussions with Marc Spiegelman and Dan McKenzie helped refine my understanding of dissipation. This work was supported by NSF grants OCE-9529878 and EAR-9219899 and by a Lamont–Doherty Earth Observatory postdoctoral fellowship. This is Caltech Division of Geological and Planetary Sciences Contribution 8801.

REFERENCES

Ahern, J. L. & Turcotte, D. L. (1979). Magma migration beneath an ocean ridge. *Earth and Planetary Science Letters* **45**, 115–122.

Asimow, P. D. & Stolper, E. M. (1999). Steady-state mantle–melt interactions in one dimension: 1. Equilibrium transport and melt focusing. *Journal of Petrology* **40**, 475–494.

Asimow, P. D., Hirschmann, M. M., Ghiorso, M. S., O'Hara, M. J. & Stolper, E. M. (1995). The effect of pressure-induced solid–solid phase transitions on decompression melting of the mantle. *Geochimica et Cosmochimica Acta* **59**, 4489–4506.

Asimow, P. D., Hirschmann, M. M. & Stolper, E. M. (1997). An analysis of variations in isentropic melt productivity. *Philosophical Transactions of the Royal Society of London, Series A* **355**, 255–281.

Asimow, P. D., Hirschmann, M. M. & Stolper, E. M. (2001). Calculation of peridotite partial melting from thermodynamic models of minerals and melts. IV. Adiabatic decompression and the composition and mean properties of mid-ocean ridge basalts. *Journal of Petrology* **42**, 963–998.

Bejan, A. (1982). *Entropy Generation through Heat and Flow*. New York: Wiley.

Budiansky, B. (1970). Thermal and thermoelastic properties of isotropic composites. *Journal of Composite Materials* **4**, 286–295.

Cawthorn, R. G. (1975). Degrees of melting in mantle diapirs and the origin of ultrabasic liquids. *Earth and Planetary Science Letters* **27**, 113–120.

Forsyth, D. W. (1992). Geophysical constraints on mantle flow and melt generation beneath mid-ocean ridges. In: Phipps Morgan, J., Blackman, D. K. & Sinton, J. M. (eds) *Mantle Flow and Melt Generation at Mid-Ocean Ridges. Geophysical Monograph, American Geophysical Union* **71**, 1–66.

Ghiorso, M. S. & Sack, R. O. (1995). Chemical mass transfer in magmatic processes IV. A revised and internally consistent thermodynamic model for the interpolation and extrapolation of liquid–solid equilibria in magmatic systems at elevated temperatures and pressures. *Contributions to Mineralogy and Petrology* **119**, 197–212.

Hart, S. R. & Zindler, A. (1986). In search of a bulk-earth composition. *Chemical Geology* **57**, 247–267.

Hirschmann, M. M., Asimow, P. D., Ghiorso, M. S. & Stolper, E. M. (1999*a*). Calculation of peridotite partial melting from thermodynamic models of minerals and melts. III. Controls on isobaric melt production and the effect of water on melt production. *Journal of Petrology* **40**, 831–851.

Hirschmann, M. M., Ghiorso, M. S. & Stolper, E. M. (1999*b*). Calculation of peridotite partial melting from thermodynamic models of minerals and melts. II. Isobaric variations in melts near the solidus and owing to variable source composition. *Journal of Petrology* **40**, 297–313.

Hofmann, A. W. (1988). Chemical differentiation of the Earth: the relationship between mantle, continental crust, and oceanic crust. *Earth and Planetary Science Letters* **90**, 297–314.

Hofmeister, A. M. (1999). Mantle values of thermal conductivity and the geotherm from phonon lifetimes. *Science* **283**, 1699–1706.

Iwamori, H., McKenzie, D. P. & Takahashi, E. (1995). Melt generation by isentropic mantle upwelling. *Earth and Planetary Science Letters* **134**, 253–266.

Kelemen, P. B. (1986). Assimilation of ultramafic rock in subduction-related magmatic arcs. *Journal of Geology* **94**, 829–843.

Kelemen, P. B. (1990). Reaction between ultramafic rock and fractionating basaltic magma I. Phase relations, the origin of calc-alkaline magma series, and the formation of discordant dunite. *Journal of Petrology* **31**, 51–98.

Kelemen, P. B. & Ghiorso, M. S. (1986). Assimilation of peridotite in zoned calc-alkaline plutonic complexes: evidence from the Big Jim complex, Washington Cascades. *Contributions to Mineralogy and Petrology* **94**, 12–28.

Kelemen, P. B., Hirth, G., Shimizu, N., Spiegelman, M. & Dick, H. J. B. (1997). A review of melt migration processes in the adiabatically upwelling mantle beneath oceanic spreading ridges. *Philosophical Transactions of the Royal Society of London, Series A* **355**, 283–318.

Kinzler, R. J., Niu, Y.-L. & Langmuir, C. H. (1993). Modal mineralogy and composition of abyssal peridotites: problems and solutions. *EOS Transactions, American Geophysical Union* **74**, 623.

Klein, E. M. & Langmuir, C. H. (1987). Global correlations of ocean ridge basalt chemistry with axial depth and crustal thickness. *Journal of Geophysical Research* **92**, 8089–8115.

McKenzie, D. P. (1984). The generation and compaction of partial melts. *Journal of Petrology* **25**, 713–765.

McKenzie, D. P. & Bickle, M. J. (1988). The volume and composition of melt generated by extension of the lithosphere. *Journal of Petrology* **29**, 625–679.

Morgan, J. P. (2001). Thermodynamics of pressure release melting of a veined plum pudding mantle. *Geochemistry Geophysics Geosystems* **2**, U1–U39.

Parmentier, E. M. & Phipps Morgan, J. (1990). Spreading rate dependence of three-dimensional structure in oceanic spreading centers. *Nature* **348**, 325–328.

Phipps Morgan, J. & Forsyth, D. W. (1988). Three-dimensional flow and temperature perturbations due to a transform offset: effects on oceanic crustal and upper mantle structure. *Journal of Geophysical Research* **93**, 2955–2966.

Plank, T., Spiegelman, M., Langmuir, C. H. & Forsyth, D. W. (1995). The meaning of 'mean F': clarifying the mean extent of melting at ocean ridges. *Journal of Geophysical Research* **100**, 15045–15052.

Presnall, D. C. (1969). The geometrical analysis of partial fusion. *American Journal of Science* **267**, 1178–1194.

Schoofs, S., Spera, F. J. & Hansen, U. (1999). Chaotic thermohaline convection in low-porosity hydrothermal systems. *Earth and Planetary Science Letters* **174**, 213–229.

Scott, D. R. & Stevenson, D. J. (1989). A self-consistent model of melting, magma migration and buoyancy-driven circulation beneath mid-ocean ridges. *Journal of Geophysical Research* **94**, 2973–2988.

Sparks, D. W. & Parmentier, E. M. (1993). The structure of three-dimensional convection beneath oceanic spreading centers. *Geophysical Journal International* **112**, 81–91.

Spiegelman, M. & Kenyon, P. (1992). The requirements for chemical disequilibrium during magma migration. *Earth and Planetary Science Letters* **109**, 611–620.

Spiegelman, M. & McKenzie, D. (1987). Simple 2-D models for melt extraction at mid-ocean ridges and island arcs. *Earth and Planetary Science Letters* **83**, 137–152.

Verhoogen, J. (1965). Phase changes and convection in the Earth's mantle. *Philosophical Transactions of the Royal Society of London, Series A* **258**, 276–283.